Frictional forces for disc-type pigging of pipelines

Hendrix, M. H.W.; Graafland, C. M.; van Ostayen, R. A.J.

DOI
10.1016/j.petrol.2018.07.076

Publication date
2018

Document Version
Final published version

Published in
Journal of Petroleum Science and Engineering

Journal of Petroleum Science and Engineering 171 (2018) 905–918

Contents lists available at ScienceDirect

Journal of Petroleum Science and Engineering

journal homepage: www.elsevier.com/locate/petrol

Frictional forces for disc-type pigging of pipelines

M.H.W. Hendrix[a,*], C.M. Graafland[b], R.A.J. van Ostayen[c]

[a] Laboratory for Aero and Hydrodynamics, Delft University of Technology, The Netherlands
[b] Shell Technology Centre Amsterdam, Amsterdam, The Netherlands
[c] Department of Precision and Microsystems Engineering, Delft University of Technology, The Netherlands

ARTICLE INFO

Keywords:
Pipeline pig
Friction coefficient
Sealing disc
Pig velocity

ABSTRACT

We investigate the frictional force which is acting on a pipeline pig. Two complementary experimental setups have been designed and used to study the sealing disc of a pig, which is responsible for the frictional force between the pig and the pipe wall. Six 12″ off the shelf sealing discs from two different vendors have been used. The first setup is a static setup in which the sealing disc is subjected to a normal wall force and a tangential friction force. A unique feature of the setup is that the ratio between the friction force and the wall force can be readily adjusted. This allows to experimentally determine the force ratio which is directly related to the Coulomb friction coefficient, which is often a difficult parameter to predict. Furthermore, the static setup is used to systematically study the effect of oversize, thickness, and Young's modulus of the sealing disc on the frictional force. A direct comparison with Finite Element (FE) calculations is made. The second experimental facility consist of a dynamic setup in which a sealing disc is pulled through a vertical 1.7 m long pipe. The effect of possible lubrication on the frictional force is studied by applying water to the sliding contact and comparing the results with dry pull tests for different sliding velocities. The corresponding difference in the Coulomb friction coefficient was quantified using FE calculations which were successfully verified with the static setup. The sensitivity of possible wear of the sealing disc on the frictional force is discussed.

1. Introduction

Pipelines that are used for the transport of fluids represent significant costs and need regular maintenance (Rui et al., 2017, 2018). In the oil and gas industry this is usually done by sending so-called pigs through the pipeline, see Fig. 1a. Such a pig travels along with the production fluids through the pipe and can serve multiple maintenance purposes. For example pigs are used to remove wax particles that may have been deposited at the pipe wall (Wang et al., 2008; Tan et al., 2014; Quarini and Shire, 2007; White et al., 2017) or to sweep out unwanted liquid accumulation in a pipeline that is used for multiphase gas-liquid transport (Wu and van Spronsen, 2005; Entaban et al., 2013). Apart from cleaning purposes, pigs can be equipped with sensors which inspect the condition of the pipe wall. This is also referred to as intelligent pigging (Quarini and Shire, 2007; Money et al., 2012). For a detailed overview of pigging applications and pig types, the reader is referred to (Cordell and Vanzant, 2003; Tiratsoo, 1992). In any case the pig is driven by the production fluids which are transported through the pipeline. This means that the pressure difference that is generated over the pig has to overcome the frictional force between the pig and the pipe wall. To ensure a safe and effective pigging operation it is thus required to know the frictional force in order to prevent too high pressures in the system.

A conventional pig completely seals the pipeline with a flexible sealing disc, see Fig. 1. The radius of the sealing disc usually has an oversize compared to the inner pipe radius, which ensures a tight seal between the pig and the pipe wall. The travel velocity of a conventional pig through a pipeline is therefore equal to the mixture velocity of the upstream fluids. In some cases it is desired to lower the travel velocity of the pig, as it may cause damage to the pipeline or the pig itself. Also for cleaning, liquid removal, and inspection purposes it is beneficial to reduce the pig velocity (Wu and van Spronsen, 2005; Money et al., 2012; Tolmasquim and Nieckele, 2008; Carvalho and Rotava, 2017). A solution to achieve a lower pig velocity without causing production loss is the use of by-pass pigs (Wu and van Spronsen, 2005). By-pass pigs have a by-pass hole which allows the production fluids to flow through the pig. As a result the pig velocity is not dictated by the upstream mixture velocity anymore, but is, in a horizontal pipe, determined by a balance of the by-passing fluid force and the frictional force of the pig with the pipe wall. The force on a by-pass pig due to the by-passing fluids has been previously studied for various by-pass pig configurations, see (Singh and Henkes, 2012; Hendrix et al., 2017). The main

* Corresponding author.
E-mail address: m.h.hendrix@gmail.com (M.H.W. Hendrix).

https://doi.org/10.1016/j.petrol.2018.07.076
Received 3 January 2018; Received in revised form 10 June 2018; Accepted 30 July 2018
Available online 07 August 2018
0920-4105/

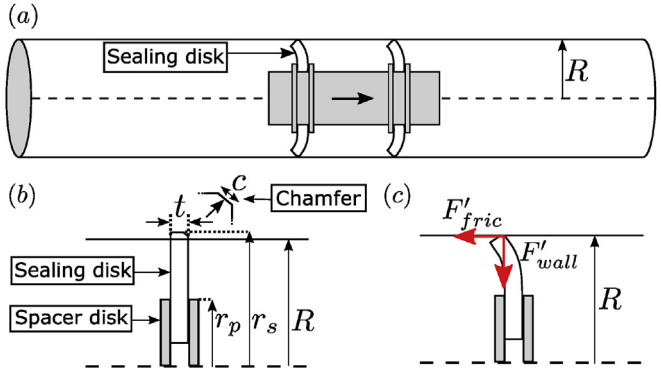

Fig. 1. (a) A pig travelling inside a pipeline (b) Undeformed sealing disk. (c) Deformed sealing disk.

focus of the current paper is on the frictional forces which are encountered during pipeline pigging. As the pig contacts the pipe wall through the sealing disc, the effect of the properties of the sealing disc on the frictional force are of interest. The external force of the pipe wall on the sealing disc is distributed along the circumference and has unit Newton per meter circumference. The distributed force can be decomposed in a distributed friction force (F'_{fric}) oriented parallel to the direction of movement of the pig and a distributed wall normal force (F'_{wall}), see Fig. 1c. At the onset of sliding the ratio of these two distributed forces gives the local Coulomb friction coefficient.

Almost no models are available to estimate the frictional force during pipeline pigging: predictions often rely on empirical findings and field experience (Cordell, 1992; Esmaeilzadeh et al., 2009). For example Cordell (1992) presents a diagram in which the driving pressure that is needed to overcome the frictional force is solely dependent on what type of pig is used (e.g. a cleaning pig versus an inspection pig). However, no information on the geometrical or material properties of the sealing disc is present in this approach. O'Donoghue (1996) presents a simplified model which does include geometrical and material properties of the sealing disc into a friction model. This model assumes that the deformed sealing disc adopts the shape of an circular arc and subsequently evaluates the internal stresses in the sealing disc which can be used to predict the frictional force. Despite that the model contains more physics than for example Cordell's model, it is known to systematically underpredict the friction force (O'Donoghue, 1996; Hendrix et al., 2016). Rather than relying on a simplified model, another approach is to perform a full Finite Element (FE) calculation of the sealing disc, which has recently been undertaken in (Zhu et al., 2015a, 2015b). Clearly, an axisymmetric 2D or even full 3D FE approach has the advantage that it contains more physics than for example a simplified axisymmetric 1D approach, such as for example the model of O'Donoghue (1996). On the other hand, it is more difficult to embed case specific FE calculations in already existing tools.

Two types of laboratory approaches to experimentally study the frictional force of a sealing disc have been found in the literature. One approach consists of a pull test in which a sealing disc/pig is pulled through a pipe while monitoring the pulling force (Zhu et al., 2015b, 2017). An advantage is that in steady state motion this pull force can be directly related to the friction force. A disadvantage is that the wall normal force is not directly measured, and therefore the Coulomb friction coefficient is unknown. Another approach relies on fixating the sealing disc while pressing it against a rotating steel plate which mimics the pipe wall, see (Tan et al., 2015) in which this setup was used to study wax removal from a pipe wall. Such a setup can be used as a tribometer in which the load and friction force can be simultaneously measured which enables to measure the friction coefficient for various contacts (Tan et al., 2013; Lan et al., 2017). While the Coulomb friction coefficient can be carefully characterized with such a setup, a disadvantage is that the friction force of a sealing disc in a confining pipe geometry is not directly measured.

In the present research a static experimental setup is presented which is used to simultaneously measure the friction force and the wall normal force acting on a sealing disc in a confining pipe geometry. The static setup is a modified and improved version of the setup described in (Hendrix et al., 2016), which will be explained in the Section 2. Six 12" off the shelf sealing discs from two different vendors have been used in the experiment. A flexible hull is wrapped around the sealing disc and F'_{wall} is subsequently generated by reducing the diameter of that hull. F'_{fric} is generated by pulling the disc in the axial direction. The forces are recorded in static equilibrium. The forces that are applied in static equilibrium are the same as for a sealing disc that moves in steady state motion through a pipeline. By changing the force ratio between the friction force and the wall force the Coulomb friction coefficient which would apply to a sealing disc which moves at steady state is thus mimicked. The experimental setup thus allows to study the effect of the friction coefficient which is difficult to study in a dynamic experiment in which a sealing disc is pulled through a pipe and the wall force is generally unknown. The results from the static setup, which is referred to as static pig pull facility, are captured by 2D axisymmetric FE calculations for which appropriate boundary conditions are formulated. A detailed comparison is made for both the involved forces as well as the shape of the deformed sealing disc. Apart from the friction coefficient, the effect of the oversize, the thickness, and the Young's modulus of the sealing disc on the friction force are investigated.

Next to the static pig pull facility, a new dynamic pig pull experiment is designed which is used to present a case example of how the results of the static pig pull facility can be related to a dynamic pull test. In this dynamic experiment the sealing disc is pulled through a 1.7 m vertical pipe while monitoring the pull force. The effect of possible lubrication by applying water at the sliding contact is investigated. The difference in friction coefficient between a dry and wet contact is quantified.

The outline of the paper is as follows. In Section 2 the experimental setup of the static and the dynamic pig pull facility and the applied measurement procedure are explained. At the end of the section the numerical setup for the FE calculations and the applied boundary conditions are discussed. Section 3 presents the results from the static pig pull facility and a direct comparison with the FE calculations is made. Subsequently the results from the dynamic pig pull facility are presented and linked to the results of the static experiments. Section 4 concludes and discusses possibilities for future research.

2. Methods

Inspecting Fig. 1b we can identify two dimensionless numbers pertaining to the undeformed geometry of the sealing disk. There is a dimensionless thickness t' and a dimensionless clamping ratio r_p', which are defined as:

$$t' = \frac{t}{r_s - r_p} \tag{1}$$

$$r_p' = \frac{r_p}{r_s} \tag{2}$$

Here t is the thickness of the sealing disc, r_s is the outer radius of the sealing disc, and r_p is radius of the spacer discs which are used to attach the sealing disc to pig body. A third geometrical dimensionless number could take the presence of a possible chamfer into account, see Fig. 1b. The dimensionless chamfer height can be for instance defined as $c' = c/t$, where c is the length of the chamfer which is for simplicity assumed to be under an angle of 45°. The effect of a variation in chamfer size is discussed in Section 3.4. Two additional dimensionless numbers can be introduced for the sealing disk which is deformed due to the confinement of the pipe wall, see Fig. 1c. We define the oversize parameter Δ and the force ratio μ as follows:

Table 1
Overview of the sealing discs used in this study. Both the geometry and the material properties of the discs are listed. One set of spacer discs is used for all experiments ($r_p =$ 86 mm).

	Disc A	Disc B	Disc C	Disc D	Disc E	Disc F
Batch	X_1	Y	X_2	X_2	X_2	X_2
r_s (mm)	163.3	161.2	155.2	155.0	154.7	155.4
t (mm)	15.9	15.2	13.6	15.5	17.4	15.4
r_p' (−)	0.527	0.533	0.554	0.555	0.556	0.553
t' (−)	0.203	0.202	0.197	0.224	0.254	0.221
Shore A hardness	75 (75.6)[b]	75 (79.6)[b]	75	75	75	65
E-modulus (MPa)	8.5	13.7	10.1[a]	10.1	10.1[a]	6.0

[a] The E-modulus of this disc is not obtained in a test, but assumed to be equal to the E-modulus of disc D. This disc is from the same batch as disc D, and only has a different thickness.
[b] Values as measured according to ASTM D2240, see Appendix A.

$$\Delta = \frac{r_s - R}{R} \times 100\% \tag{3}$$

$$\mu = \frac{F'_{\text{fric}}}{F'_{\text{wall}}} \tag{4}$$

Here R is the inner pipe radius, F'_{fric} is the distributed friction force and F'_{wall} is the distributed wall normal force. Most sealing discs are made of polyurethane. This elastomer has a high abrasion resistance, tear strength and resistance to hydrocarbons (O'Donoghue, 1996). The chemical composition of the sealing disc is proprietary to the manufacturer of the pig and it influences the Young's modulus of the material, which is also referred to as E-modulus. The E-modulus is usually an input parameter for deformation models. Unfortunately, manufacturers do not specify the E-modulus of their product. Instead they specify the Shore A hardness, which is a measure of the resistance of a material to indentation. Typical values for the Shore A hardness of sealing discs are in the range of 60–85 ((Cordell and Vanzant, 2003)).

In this study a total of six sealing discs have been studied, see Table 1. These discs have been obtained from two different pigging vendors, here anonymously named X and Y. The discs from both vendors are intended for pigging of 12″ pipelines. From vendor X, three different batches were obtained: X_1, X_2, and X_3. The Shore hardness as specified by the manufacturer is listed. As the E-modulus was not specified it was determined by material tests. These tests consisted of a stress strain analysis using representative dog bone samples from the disk. In addition to the stress strain tests, the Shore hardness of disc A and disc B was determined. A value of respectively 75.6 and 79.6 was found, which are put in between brackets in Table 1. The value of disc A is within the specification of the manufacturer, but the value of disk B is slightly higher. The details of the material tests can be found in Appendix A. In any case it is clear that the value of the specified Shore hardness cannot be used to deduce the E-modulus, for example by using the Gent equation (Gent, 1958), as discs with the same specified Shore hardness turn out to have different values for the E-modulus. The radius of the spacer discs is kept constant in the experiments and is equal to 86 mm. All experiments have been performed at room temperature.

Disc A and disc B are the main discs that are used in our experiments. They have similar properties except that they come from a different vendor and have a different E-modulus. Disc C, D, and E are from the same vendor and from the same batch. They have similar properties, except for the variation in the thickness of the discs. These discs are used to study the effect of the thickness on the friction force. Discs C and disc F have similar properties except for the E-modulus. These discs are thus used to study the effect of the E-modulus on the friction. The effect of the oversize Δ and of force ratio μ are investigated for all the disks, as the experimental setup is designed to easily vary these

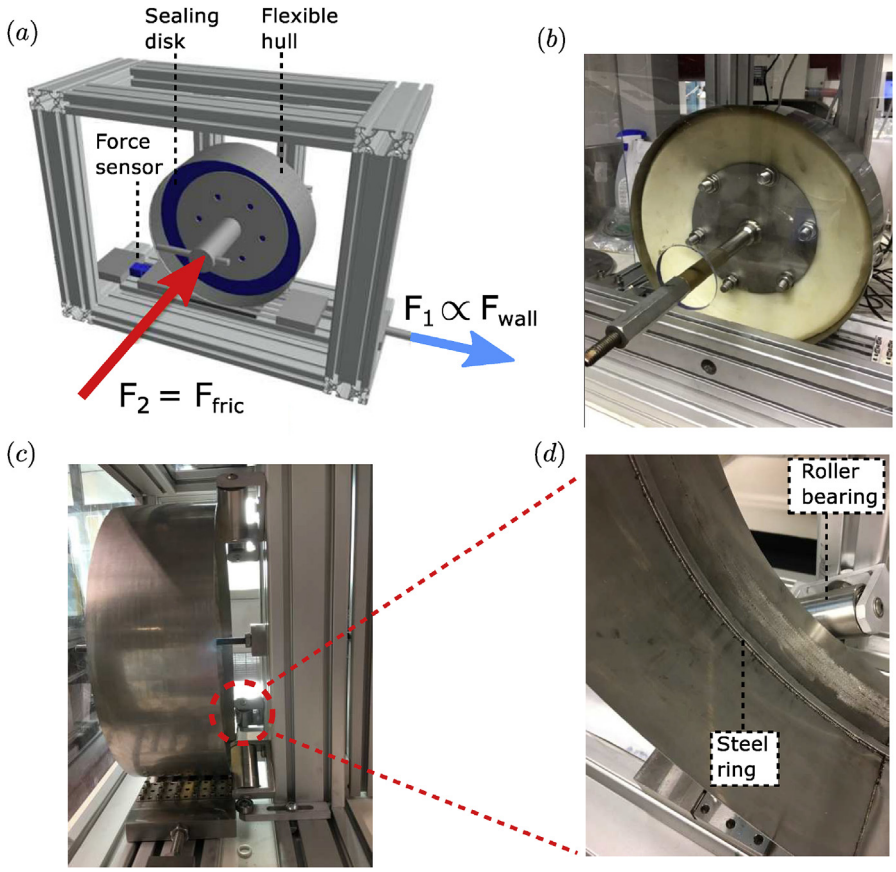

Fig. 2. (a) Schematic of the setup. (b) Front view of the setup. (c) Side view of the setup. (d) Close-up of the steel ring and roller bearing.

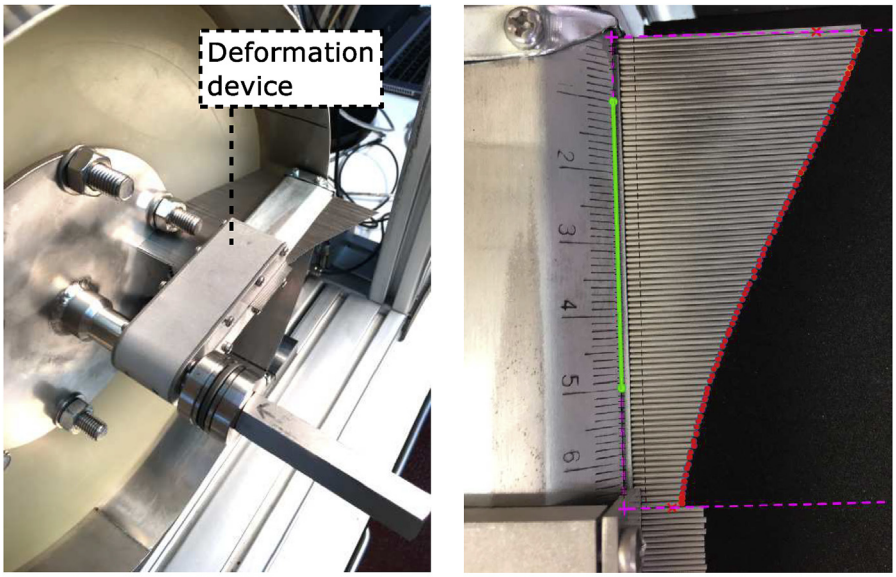

Fig. 3. (a) Profile comb. (b) Deformation extracted from the profile comb.

parameters, which will be explained in the next section.

2.1. Static pig pull facility

Deformation of the sealing disc is caused by the external forces F'_{wall} and F'_{fric}. In static equilibrium these forces are balanced by internal stresses in the polyurethane disc. The ratio of the external forces F'_{fric} and F'_{wall} gives the force ratio μ, see equation (4). This force ratio would be equal to the Coulomb friction coefficient of a sealing disc which moves at steady state through a pipeline on which the same forces act. The friction coefficient is a difficult parameter to predict, since it depends on both the material properties of the sealing disc and the local conditions of the inner pipe wall. Furthermore, it also depends on the type of fluids that are being transported, as these fluids may act as lubricant which can decrease the friction coefficient (Tan et al., 2013; Persson, 1998). Instead of trying to predict this force ratio, an experiment is designed in which the force ratio can be imposed, see Fig. 2. The experimental setup is a modified version of the setup presented in (Hendrix et al., 2016) and works as follows.

The setup consists of a flexible hull which is wrapped around the sealing disk, see Fig. 2a. By applying a force F_1 on the hull, the diameter of the hull will be reduced. As a result the sealing disk will deform and the corresponding force F_1 is recorded by a force sensor. The diameter reduction of the hull mimics the confinement of the pipe wall which determines the oversize parameter Δ, see equation (3). The oversize can thus be easily varied by changing the diameter of the hull. We define the magnitude of the distributed wall force and friction force integrated along the edge of the pipe as F_{wall} and F_{fric} respectively:

$$F_{wall} = 2\pi R|F'_{wall}| \tag{5}$$

$$F_{fric} = 2\pi R|F'_{fric}| \tag{6}$$

The unit of F_{wall} and F_{fric} is Newton. By applying the principle of virtual work, F_{wall} can be related to the circumferential force F_1:

$$\begin{aligned} F_{wall}\,\mathrm{d}r &= F_1 2\pi \mathrm{d}r \\ F_{wall} &= 2\pi F_1 \end{aligned} \tag{7}$$

Here r represents the radial coordinate. A second force F_2 is generated by displacing the centre of the disc in axial direction, see Fig. 2a/b. The force sensor which records F_2 is located at the back of the setup. This force is equal to the friction force F_{fric} in the axial direction between the hull and the sealing disc:

$$F_{fric} = F_2 \tag{8}$$

The force ratio can now be expressed in terms of F_1 and F_2:

$$\mu = \frac{F_{fric}}{F_{wall}} = \frac{F_2}{2\pi F_1} \tag{9}$$

By changing F_2 and F_1 the force ratio can be readily varied. In order to be able to obtain higher values of the force ratio as compared to (Hendrix et al., 2016), a 2 mm steel ring has been welded onto the hull in the circumferential direction, see Fig. 2d. This ring prevents that the disc slides in the axial direction when F_2 is increased.

A side view of the setup is shown in Fig. 2c. Here it is visible that the back of the flexible hull is supported by roller bearings which are mounted on the frame. Fig. 2d shows a close-up of one of the six roller bearings which are used. The addition of roller bearings is an improvement compared the setup as presented in (Hendrix et al., 2016). The roller bearings ensure that very little friction exists between the hull and the frame. This is especially important when the axial force F_2 is increased, which effectively pushes the hull against the roller bearings. Without the roller bearings a friction force between the hull and the frame could exist which would result in an under prediction in the value of F_1. The setup is operated in such a way that static equilibrium is reached. The corresponding values for F_{fric} and F_{wall} in this static situation represent the same force balance that would apply to a sealing disc on a pig that moves in steady state motion in a pipeline.

Next to the forces that act on the sealing disc also the deformation of the sealing disc is measured. This is done by mounting a profile comb on the spacer disc, see Fig. 3. The profile comb is subsequently pressed against the sealing disc in order to measure the shape. The rotation of the profile comb can be adjusted which allows to measure the deformation at different positions. Deformation measurements in addition to force measurements provide a more complete set of results compared to force measurements alone, as was done in (Hendrix et al., 2016). Fig. 3a shows the profile comb in a 3 o'clock position, but also the 12 o'clock and 6 o'clock position have been employed. These different positions allow to verify if the deformation of the sealing disc is axisymmeteric. A camera holder is used to take a photo in the same plane as the profile comb. Subsequently the deformation is obtained by extracting the position of the pins using image processing. The detected location of the pins is shown by the red dots in Fig. 3b. Even though this

study focuses on pigs with a sealing disc, the experimental setup could be used to study other types of pigs, such as pigs with cups or foam pigs (Quarini and Shire, 2007). In case of foam pigs it however makes less sense to attempt to measure any deformation in axial direction, as a foam pig is mainly compressed in radial direction. In the next section the measurement procedure and a typical result obtained from the force sensors are discussed.

2.1.1. Measurement procedure

The measurements were performed with two 24-bit GSV-2TSD-DI data acquisition devices connected to a 1 kN and 2 kN load cell (KD40S, ME-Systeme) which record the circumferential force F_1 and the axial force F_2, respectively. The measurements were performed at a sample frequency of 10 Hz and logged onto a computer. The procedure of a typical measurement is as follows. First, the disc is brought to a specific oversize by applying a force F_1 which reduces the diameter of the hull. The oversize is kept fixed within one experiment. Subsequently, the disc is step-wise displaced in axial direction resulting in a force F_2. One step corresponds to a rotation of the screw that can be seen in Fig. 2b. The lead of the screw is 1.5 mm. One rotation is made in approximately 30 s to maintain static equilibrium. The axial force F_2 is increased up to a predetermined maximum which is just below the value which would result in the disc moving over the steel ring, see Fig. 2d. After reaching a maximum value, F_2 is decreased in steps to come back at a value of 0 N. This procedure is repeated three times per measurement. Fig. 4a shows one typical time series of measurement data which were obtained by applying the procedure to disc B subjected to an oversize $\Delta = 4\%$.

Fig. 4a clearly shows the stepwise behaviour in the forces, which corresponds to the stepwise adjustment of F_2 as explained above. It is noted that an increase in F_2 corresponds to a decrease in F_1 and vice versa. This is expected as the disc is not only deformed by a wall normal force (related to F_1), but also by a friction force (equal to F_2). The corresponding value of the force ratio μ according to equation (9) is included in Fig. 4a. For the axial force F_2 three zones can be distinguished: a rise zone, where F_2 increases, a rest zone, where F_2 does not change and a relax zone, where F_2 decreases. The rest zone lasts longer and is noisier compared to when F_2 is increasing, because here the profile comb is used to determine the deformation at three different positions on the sealing disc: 12 o'clock, 3 o'clock and 6 o'clock.

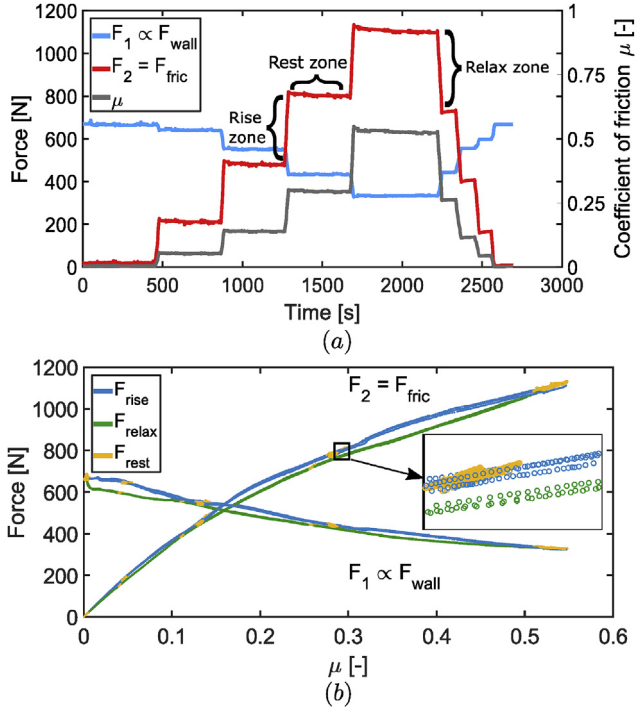

Fig. 4. (a) Time series of typical force data and corresponding force ratio as obtained in the experiment. (b) Force data plotted as function of the force ratio μ. A close-up of the data between μ equal to 0.29 and 0.31 is included.

Fig. 4b shows an alternative way of plotting the same data. The forces F_1 and F_2 are now plotted as function of μ. The data are colour coded to distinguish between the rise, relax, and rest zones. In this plot now all three time series of the measurement are included. The inset in Fig. 4b shows a close up of the data. The data from the three data sets are very close to each other, which thus confirms the excellent reproducibility of the experiment. It can also be seen that the data from the relax zone, as shown in blue, differ from the data from the rise zone, which points out that a small hysteresis is present in the experiment.

A total of six different sealing discs have been used in the experiments as listed in Table 1. Disc A and disc B were tested at four oversizes: 1%, 2%, 3% and 4%. Deformations were measured for disc A and disc B. Similar sets of experiments are conducted for disc C till disc F at oversizes of 3% and 4%. Deformations are not measured for these discs. Comparing the results for disc C,D and E will show how the thickness affects the friction force at different μ values, as the discs are identical except from their thickness. Comparing the results of disc D and disc F will show how the E-modulus affects the friction force at different μ values, as these discs are identical except for their E-modulus. The results of the static measurements will be presented and discussed in Sections 3.1 and 3.2.

2.2. Dynamic pig pull facility

To study the dynamic friction force a new dynamic pig pull facility has been designed, see Fig. 5. The setup consists of a 1.7 m vertical carbon steel pipe through which a sealing disc can be pulled at a preset velocity using a linear actuator. The inner radius of the pipe is 157 mm. The linear actuator (Thomson, ECT130) is connected to a brushless AC servomotor (AKM63), which is located at the top end of the pipe. The actuator is able to translate a spindle which has a total length of 2 m and a lead of 20 mm. At the lower end of the spindle a 5 kN load cell (AXH Scaime) is connected to which the sealing disc is attached, see Fig. 5a/b. The load cell is able to directly measure the propulsive force which is needed to pull the sealing disc through the pipe. Simultaneously the position, velocity and acceleration are monitored with a logging frequency of 200 Hz. The speed of the sealing disc can be varied between 5 and 300 mm/s. The pipeline is placed vertically which makes it possible to add liquids uniformly on top of the sealing disc, see Fig. 5a. Herewith the effect of possible lubrication on the frictional force caused by the presence of a liquid can be investigated. For a sealing disc moving in an upwards direction in the pipe, the steady state force balance reads:

$$F_m = F_{\text{fric}} + F_g \tag{10}$$

where F_m is the propulsive force of the servomotor, F_{fric} is the friction force between the sealing disc and the pipe wall and F_g is the gravitational force. In dry experiments F_g is due to the mass of the sealing disc and of the spacer discs. In wet experiments also the mass of the lubricant supply on top of the disc has to be taken into account.

A by-pass is created by drilling three holes in the spacer discs, see Fig. 5a. For the wet experiments, this allows the lubricant to flow through the disc into the leakage tray when the liquid level equals the height of the upper spacer disc. With a minimum amount of lubricant a wet sliding contact can be obtained.

2.3. Measurement procedure

Rather than a parameter study, as is conducted with the static pig pull facility, only one disc (disc A) is used in the dynamic pig pull experiments as case study. A measurement commences with the spindle in its most extended position with the sealing disc mounted on it (approximately

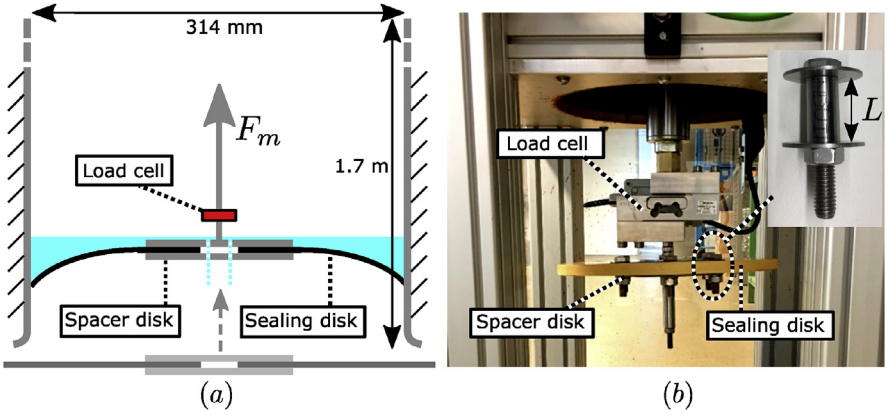

Fig. 5. (a) Schematic of the dynamic pig pull facility (b) Photograph of the dynamic pig pull facility.

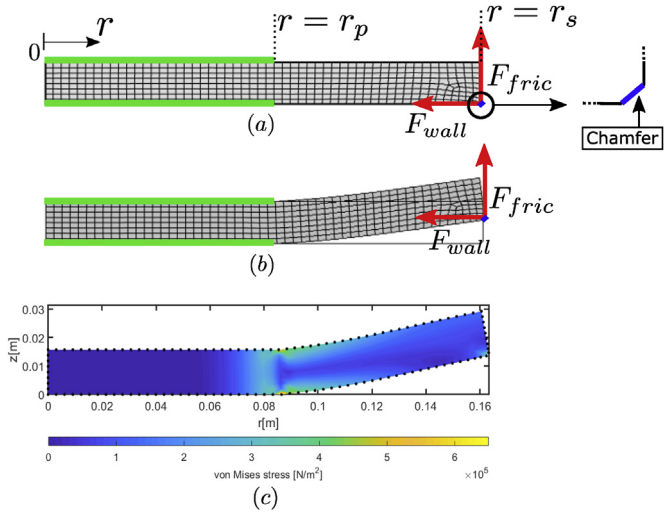

Fig. 6. Geometry and boundary conditions of the finite element model. (a) Initial geometry. (b) Deformed geometry. (c) Typical simulation result.

30 cm below the pipe), see Fig. 5b. This is called the home position of the disc. From here the sealing disc is pulled slowly at a velocity of 5 mm/s to the initial position, which is 50 mm into the pipe. The disc is kept in this position for 60 s to make sure that possible settling effects are no longer present. After this delay time the actual pull test begins and the disc accelerates, moves up through the pipe at the preset velocity, and then decelerates until rest in its final position at the top of the pipe. Three preset velocities have been used: 100, 200, and 300 mm/s. The spindle acceleration and deacceleration are set to 100 mm/s^2. When the disc is moving up, both the motion (position, velocity, and acceleration) and the propulsive force are monitored. No data are logged when the disc moves back down, as only pull tests are considered in this study.

In the wet experiments an additional step is added to the procedure. After the disc is positioned in the start position, water is inserted from a small tap at the top of the pipeline until it starts leaking through the by-pass holes, see Fig. 5a. The top part of the sealing disk and the adjacent pipe wall are now wetted. Subsequently, the tap is closed and the leakage tray is emptied before it is put back under the pipe. The pull test can now begin. When the disc is moving upwards the water leaking past the sealing disc or through the by-pass holes is negligible. In this way it is thus possible to create a wet contact between the pipe wall and the sealing disc. At the end of the pull test the disc is returned back to its start position. When the disc starts moving down it buckles to the opposite side and as a result the water flows through the by-pass holes and is collected into the leakage tray. The mass of the water (approximately 1 L in volume) is determined and used in the force balance, see Equation (10). In this study only water is used as lubricant.

The two spacer discs are separated by a small length of tube, and this tube therefore determines how tight the sealing disc is clamped between the spacer discs. Three configurations are created by selecting three values for the length L of the tube which is shown Fig. 5b. To the best knowledge of the authors the effect of this parameter on the frictional force of a sealing disc of a pig has not been reported in previous studies. As will become clear in Section 3.3 the length L of the tube influences the outer diameter of the sealing disc, and therefore the oversize, due to the nearly incompressible behaviour of the polyurethane. For all three configurations wet and dry experiments are conducted at varying speeds. Each separate experiment is repeated five times for reproducibility purposes; the first two runs are used to mitigate any settling effects of the disc and the last three runs are used in the actual analysis. Next to the varation of L the disc is placed in both a face up and face down orientation to investigate the presence of any possible asymmetries.

2.4. Finite element model

Comsol Multiphysics (version 5.2) is used in this study for the Finite Element (FE) analysis. We solve the structural mechanics problem in which we solve for the deformation of the sealing disc which is caused by the wall force and the friction force which act on the chamfer of the sealing disc, see Fig. 6. We consider static equilibrium, in which case Newton's second law reads:

$$\nabla \cdot \sigma = 0 \tag{11}$$

Here σ is the Cauchy stress tensor. The stresses are calculated using a linear isotropic material model. The E-modulus which is used has been determined by material tests and can be found in Table 1. The Poisson's ratio ν is taken equal to 0.49. Since the typical deformation which occurs can be in the order of a few times the thickness of the sealing disc, a nonlinear geometry model is used. We assume an axisymmetric geometric model.

Fig. 6 shows the typical mesh which is used for the calculations. Second order quadratic elements are used. The meshing is adapted on the thickness of the disc to guarantee appropriate meshing for both thick and for thin discs. In the thickness direction the size of the element is controlled between a minimum size of t/6 and a maximum size of 1.2 times t/6. In the radial direction the edges have a length equal to the edges in the thickness direction multiplied by a factor 1.5. The mesh consists of approximately 400 elements, which was verified to be sufficiently fine by making a comparison with simulation results with a smaller number of elements.

The green lines in Fig. 6 represent roller boundary conditions on both sides of the sealing disc between $r = 0$ and $r = r_p$, due to the spacer discs. Here the sealing disc is constrained to move in the normal

direction, but it is allowed to move parallel to the spacer discs. The freedom to move, however, is limited, due to the axisymmetric geometry. It was found that this boundary condition is appropriate to model the confinement of the spacer discs, even though a finite, non-zero clamping force of the spacer discs on the sealing disc exists. An alternative boundary condition could be a completely clamped boundary condition (Nieckele et al., 2001), which would prohibit any movement of the disc in the region of the spacer discs. This was found to be unsuitable, as a finite deformation was observed in the region of the spacer discs, which will become clear in Section 3. The blue square represents the chamfer of the disc, where the wall force and the friction force act. The chamfer size c is set to 1.4 mm, as measured from the sealing disc. The remaining edges have a free boundary condition.

For low μ values high wall forces are involved when a sealing disc is confined inside a pipe. In reality and in the experiments in this study a sealing disc automatically buckles backwards with respect to the moving direction. To ensure that in the FE model the disc buckles to the correct side the FE model is solved in multiple steps. First the friction force is added and then the wall force is increased in steps to its final value. Within the solution process, the result of the previous calculation step is used as an initial condition for the next calculation step. This helps to buckle the disc in the direction of the friction force. Fig. 6c shows a typical simulation result of disc A subjected to a wall force $F_{\text{wall}} = 400$ N and a friction force $F_{\text{fric}} = 200$ N. The interior of the disc is colour coded by the von Mises stress. High stress points typically occur near the outer edge of the spacer discs.

3. Results

In this section the results are presented which are obtained by the methods described in the previous Section 2. First the results from the static experiment are presented. In Section 3.1 the deformations obtained in the experiments and the deformations found using the FE model are compared for disc A and disc B, see Table 1. In Section 3.2 the friction force as a function of μ and oversize is shown, both for disc A and for disc B. In addition, Section 3.2 shows the friction force for different values of the E-modulus and the thickness of the disc. For this purpose discs C to F are used. Section 3.3 present the results which are obtained with the dynamic pig pull experiment. Section 3.4 discusses how the results from the static and dynamic pig pull experiments are related.

3.1. Shape comparison

We have obtained the shape of the sealing disk using the deformation device as described in Section 2.1. Fig. 7 shows the results for disc A subjected to 3% oversize. In Fig. 7a a time series is shown, where the blue line denotes the wall force F_{wall} and the red line denotes the friction force F_{fric}. In the first five rest zones, where the forces are constant, the deformation of the disc is measured. To show how the measured shapes compare with the FE model, data from the last three rest zones are shown in Fig. 7b–d. The last three rest zones which correspond to subfigure b-d are indicated in Fig. 7a.

It can be seen that the FE results, which are shown by the black dots, agree very well with the average measured deformation. The FE results were obtained by applying the forces that were measured in the experiment to the chamfer of the disc in the FE model, as described in Section 2.4. It can also be noted from the measured data that the sealing disc does not deform perfectly axisymmetrically in the hull. The largest deflection occurs when the deformation device is at 6 o'clock, followed by 3 o'clock and 12 o'clock. This is a consequence of the position of the tensioning mechanism located at 6 o'clock, see Fig. 2a. This breaks the axisymmetry of the hull, resulting in a slightly non perfect circular shape. No attempt has been made to correct this, since adding new forces to the system was not desired. The gravity force is assumed to play a minor role as it is only a small fraction of the encountered wall forces.

In Fig. 7b–d the force ratio μ varies from 0.14 to 0.64 which corresponds to a substantial variation in F_{wall} and F_{fric}, see Fig. 7a. The deformation of the disc during this process, however, only changes slightly. Both the measured data from the deformation device and the FE model show this behaviour. This means that there exists approximately one axisymmetric shape of the sealing disc which is fitted in a pipe, and that the effect of μ on the final shape is only minor. As was discussed in Section 2.4 a roller boundary condition was chosen to represent the confinement of the spacer discs. It can be clearly seen that the angle of deformation is not zero at the radius of the spacer disc $r = r_p$, which supports the choice of a roller boundary condition over a fully clamped boundary condition.

The deformation results for disc A at 3% oversize were shown in Fig. 7 as case example. The deformations results of disc A for all oversizes 1%, 2%, 3%, and 4% are presented in Fig. 8a. Here the maximum deformation w_{max}, which occurs at the tip of the disc is selected, see Fig. 7d, and is plotted as function of μ.

The experimental data in Fig. 8a are plotted as error bars in different colours which correspond to different oversizes. The lower and upper limit of the error bar represent the deformation measurements at 12 o'clock and 6 o'clock, respectively, while the main data point (open circle) of the error bar represents 3 o'clock, see Fig. 7. The green error bars connected with the black line in Fig. 8a link to the deformation results in Fig. 7, as here an oversize of 3% was shown. The black line shows that w_{max} only increases by a few millimetres while μ increases significantly. At every oversize the experiment was conducted three times. The fact that the three corresponding error bars are lying on top of each other indicates that the experiment is reproducible. The same procedure was applied to disc B. These results are summarized in Fig. 8b. It can be concluded that the FE model is able to predict the shapes and w_{max} obtained in the experiment. Only for small μ no FE data are plotted. Here the FE model returns a solution buckled to the other side. In general it is found that μ does not have a large effect on how the disc is fitted in the pipeline. It is evident that the oversize does have a large effect on the shape, as a larger oversize means that the disc has to deform more to fit in the pipe. The length of the error bars in Fig. 8b is longer, indicating that there is a larger spread between the deformation measurements at 3, 6 and 12 o'clock. This can be explained by the larger E-modulus of disc B, as this stiffer disc is more sensitive to any asymmetries in the setup. The results in Figs. 7 and 8 are obtained without using a fitting parameter for the E-modulus. The E-modulus used in the FE model is shown in Table 1 and is obtained in stress and strain tests as described in Table 1. In the next section various parametric studies are described, in which also the effect of a variation in the E-modulus on the friction force is discussed.

3.2. Parameter study

Fig. 9 shows the friction force in the rise and rest zones as function of the force ratio μ for the four oversizes for disc A and disc B. The corresponding wall force F_{wall} can be obtained as the ratio of F_{fric} and μ.

A first inspection of Fig. 9 shows that the friction force of disc B is overall higher than the friction force of disc A. This is a consequence of the higher E-modulus of disc B compared to disc A, see Table 1. The maximum μ values obtained differ per oversize and per disc, indicating that the discs start to move over the steel ring (Fig. 2) at a different critical value of μ. The generic trends observed for all oversizes are similar for both discs. We focus on the μ regime between 0.2 and 0.6.

In the chosen μ regime also FE simulation results are shown in black. The black lines are fitted through 10 data points. For these data points at different μ the friction force (and thus the wall force as μ is fixed) is increased until the FE model reaches the same oversize (1–4%) as in the experiment. The shaded regions around the black lines show the results of a variation by ± 5% of the E-modulus used in the FE model.

The friction forces necessary to bring the disc in the desired oversize in the FE model correspond very well to the experiments. Both the trend

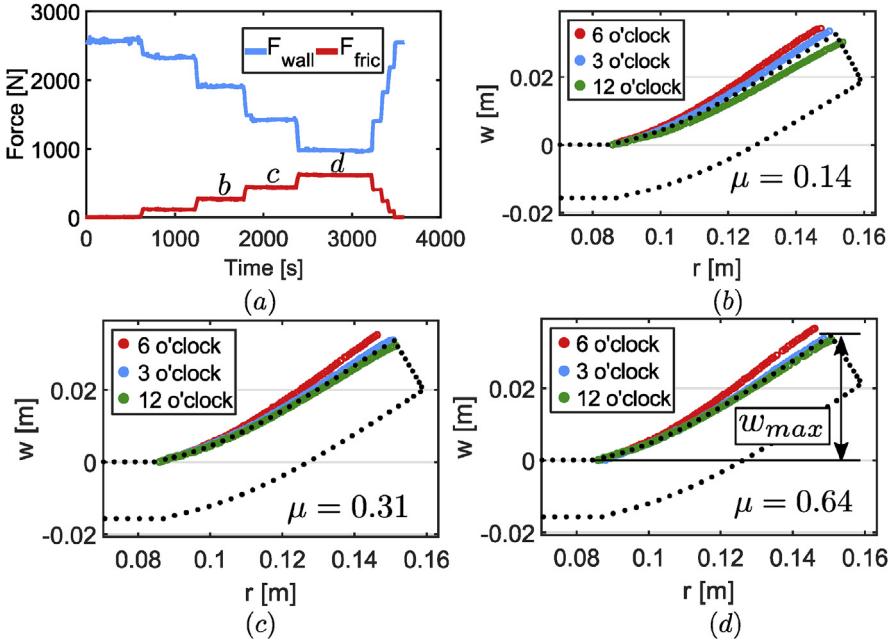

Fig. 7. Experimental results for disc A at 3% oversize. The black dotted shape in sub-figures b-d represents the FE model. (a) A time series showing the wall force and the friction force. Deformations are measured in the rest zones labeled b-d. (b) F_{wall} = 1908 N and F_{fric} = 266 N. (c) F_{wall} = 1429 N and F_{fric} = 439 N. (d) F_{wall} = 977 N and F_{fric} = 620 N.

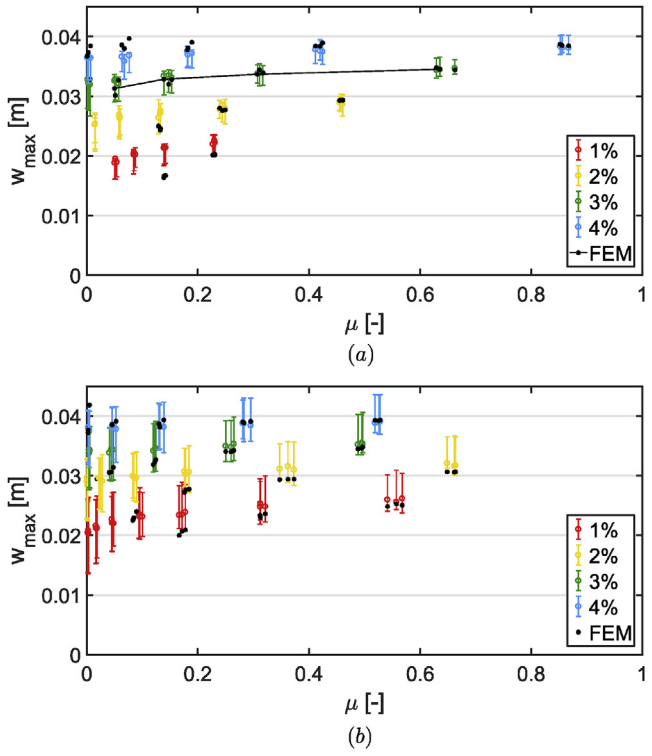

Fig. 8. Comparison of w_{max} in the experiments and in the FE model for different oversizes. (a) Disc A. (b) Disc B.

and the actual magnitudes are captured accurately by the FE model. Fig. 9a shows that the experimental results and the FE results agree very well for disc A with oversizes 2% and 3%. The FE model predicts a lower friction force to bring the disc in 4% oversize. The maximum deviation at 4% oversize is only 9.3%. At 1% oversize no experimental data are available in the chosen μ regime. For disc B, shown in Fig. 9b, the results are in agreement for the 1% and 2% oversizes. For the 3% and 4% oversizes the FE model underpredicts the friction force, with a maximum underprediction by 5.2% and 11.6%, respectively.

Both Fig. 9a and b shows that the experimental friction force data are approximately evenly spaced when the oversize increases from 1% to 4%. For the FE data the increase in friction force seems to decrease as the oversize increases. A reason for this difference in behaviour might be that the wall force is incorrectly captured at higher oversizes (and thus higher friction forces) in the experiments. To capture the wall force correctly six ball bearings were added to the setup, see Section 2.1. This was to make sure that no undesired forces were added in the plane of the hull, affecting F_1. For high friction forces the contact between the hull and the ball bearings connected to the frame may still not be completely frictionless. Undesired friction between the hull and the frame is difficult to prevent completely. Therefore the force sensor monitoring F_1 may overpredict the wall force. This means that μ is underpredicted for the experimental data in Fig. 9. There is no reason to assume that the experiment does not capture the friction force correctly. When this hypothesis is true the experimental data would shift to the right for high friction forces. Intuitively, the FE data make sense as one may expect that it is easier to increase the oversize from 3% to 4% than from 1% to 2%. This is also what has been observed in other research (Nieckele et al., 2001; Zhu et al., 2015b). To directly see the effect of the oversize on the friction three values of μ have been highlighted in Fig. 9a and b. Along these lines of constant μ experimental data have been gathered in a range between $\mu + 0.002$ and $\mu - 0.002$. The error bar represents the standard deviation of the data within this range.

Disc D and disc F are tested to see how the friction force behaves as a function of the E-modulus. Fig. 10a shows the results when the disc is at 3% oversize and Fig. 10b for 4% oversize.

The discs have similar specifications except for the Shore hardness and the E-modulus, see Table 1. The thickness and the sealing disc radius are not exactly the same; therefore in the FE model the average thickness and radius are selected. The results are shown for three different values for μ. For the disc with the lower Shore hardness and E-modulus (disc F) the experimental data agree very well with the FE data for all three values of μ. The maximum deviation in friction force between the FE results and the experiments equals 6.5%. The results of the experiments with the stiffer disc show higher

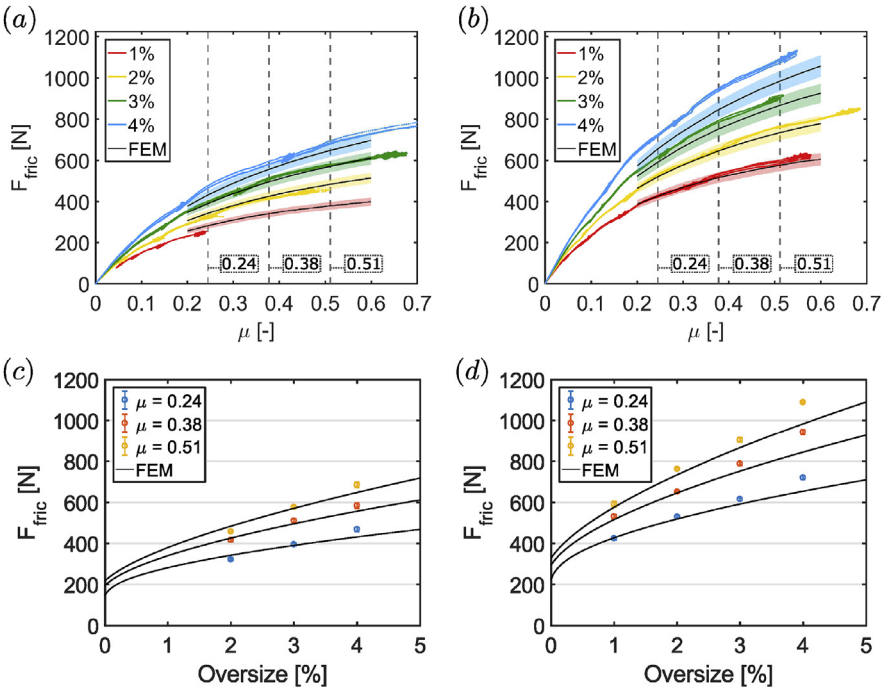

Fig. 9. (a) Friction force as a function of μ for different oversizes for disc A (b) Idem disc B. (c) The friction force as a function of the oversize for disc A (d) Idem disc B.

friction forces than predicted by the FE model, especially at 4% oversize. The maximum deviation in friction force between the FE results and the experiments equals 14.7%. This is in line with the observation in the previous section that F_{wall} is not captured correctly in the experiment for high friction forces. When F_{wall} is overpredicted, μ is underpredicted. Fig. 10 shows that lower μ values would correspond to a smaller gradient in the experimental data. It is worth mentioning that the experimental setup which is designed can actually serve as a tool to predict the E-modulus of a sealing disc in a non destructive way by fitting the experimental data on the FE results.

Disc C, disc D and disc E are tested to see how the friction force behaves as a function of the disc thickness. The discs have the same manufacturer and are from the same batch. Only the thickness of the discs is different, see Table 1. Therefore the E-modulus of disc C and disc E have not been obtained in a stress and strain test, but are assumed to be equal to the E-modulus of disc D.

Fig. 10c shows the friction force with μ being equal to 0.42. Experimental data are shown at 3% and 4% oversize. The FE model is shown for an oversize of 1%, 2%, 3% and 4%. The maximum deviation

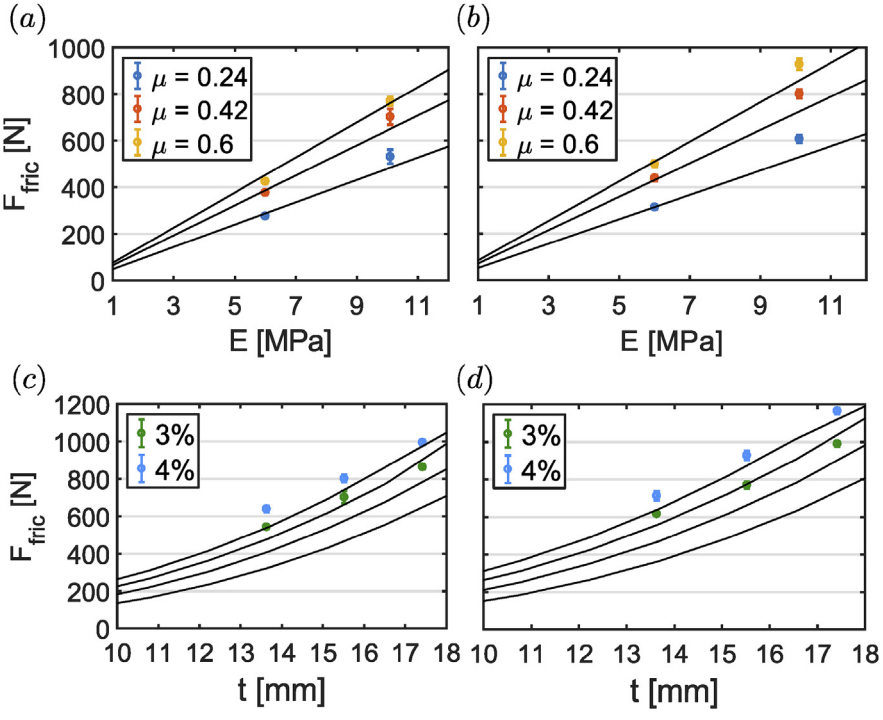

Fig. 10. The black line represents results from FE calculations. (a) The friction force as a function of the E-modulus at 3% oversize (b) The friction force as a function of the E-modulus at 4% oversize. The experimental results are compared to the FE results at three μ values: 0.24, 0.42 and 0.6. (c) The friction force as a function of the thickness at μ equal to 0.42. (d) The friction force as a function of the thickness at μ equal to 0.6. Disc C, disc D and disc E are tested at 3% and 4% oversize. The FE results correspond to, from top to bottom, 4%, 3%, 2% and 1% oversize.

in friction force between the FE results and the experiments equals 18.1%. This deviation occurs for disc C at 4% oversize. Fig. 10d shows similar data with μ equal to 0.6. Here the maximum deviation in friction force between the FE results and the experiments equals 11.2%, also occurring for disc C at 4% oversize. For the two thicker discs the FE model agrees very closely with the experimental data while the friction forces for the thinnest disc are underpredicted.

3.3. Results from dynamic pig pull experiments

In this section the experimental results from the dynamic pig pull experiments are presented. All experiments are conducted with disc A. As was discussed in Section 2.3 the length of the tubes L which defines the distance between the spacer discs was varied. Thereby the clamping force of the spacer discs which squeezes the sealing disc is varied. The reduction in the length compared to the original length when the clamping force is zero is defined L'. Three values for L' have been studied: 0, 1, and 2 mm. As the original thickness of disc A is equal to 15.9 mm (see Table 1), values of L' equal to 0,1, and 2 mm correspond to a compression of 0%, 6%, and 13% respectively. The compression in the axial direction causes the disc to expand in radial direction, due to the nearly incompressible behaviour of polyurethane. As a result the outer diameter increases. This has been quantified, see Table 2. Here it can be seen that for $L' = 0$ the original radius of the disc equals $r_s = 162.2$ mm. As the inner radius of the pipe is 157 mm, this corresponds to an oversize of $\Delta = 3.33\%$. Upon increasing the clamping force by increasing L' the radius and corresponding oversize thus increase.

For the tubes that squeezed the disc by 1 mm or 2 mm the disc oversizes were slightly higher after a first pull test, compared to the oversize measured directly after assembling the spacer discs on the sealing disc. For the tubes that were not squeezing the disc ($L' = 0$ mm) this phenomenon was not observed. This indicates that a small settling effect is present which can be explained by the forces that occur in the experiment that are able to pull the disc radially outward. When the clamping force is zero ($L' = 0$) the disc is able to retract to its original position, but with a non zero clamping force ($L' = 1$ and $L' = 2$) the disc remains radially extended. This settling effect is not investigated further in this work.

The effect of L' on the frictional force is investigated for various disc speeds. Also the effect of a dry versus a wet contact is investigated, as described in Section 2.3. The experiments and corresponding parameters are summarized in Table 3. Here it is also shown that also a face up and face down orientation of the disc is distinguished. The average values of the force data are listed as found when the disc is moving at constant velocity, as described in Section 2.3. The sequence of the experimental runs can be deducted from the table: first the runs without squeezing are conducted, followed by the runs with 1 mm and 2 mm squeezing. For one set of tubes we start with the dry runs: first five runs at 100 mm/s followed by five runs at 200 mm/s and 300 mm/s. After this, the dry face down, wet face down and wet face up runs are performed. Before the experiments with the next set of tubes are conducted, the setup is left for an entire day to dry. The experiments in Table 3 correspond to approximately 600 m of pipeline pigging (three sets of tubes, four configurations, three speeds, five repetitions, 3.2 m between subsequent pull tests). The values in Table 3 are average values based on the last three runs from each set of five runs, as the first two runs are done to mitigate any settling effects.

Table 2
Oversizes before and after a first pull test.

L' [mm]	Before pull test		After pull test	
	r_s [mm]	Δ [−]	r_s [mm]	Δ [−]
0	162.2	3.33	162.2	3.33
1	162.7	3.64	162.9	3.74
2	163.3	4.04	163.7	4.24

Table 3
Experiments performed with three sets of tubes: 0 mm (no squeezing), 1 mm and 2 mm. The mean values of the force data are tabulated, averaged over three runs and as found when the disc is moving at constant velocity. In addition, the standard deviation for this period is added between brackets. In total the runs correspond to 600 m of pigging distance.

L' [mm]	Speed [mm/s]	Friction force [N]			
		Dry, face up	Dry, face down	Wet, face down	Wet, face up
0	100	819 (1.2)	815 (1.9)	680 (9.7)	702 (3.9)
	200	824[b] (1.4)	814 (1.3)	682 (5.3)	710[b] (2.3)
	300	830 (1.2)	815 (1.0)	685 (1.2)	713 (2.1)
1	100	843 (2.4)	828 (3.1)	701 (3.6)	717 (1.8)
	200	845[b] (2.2)	828 (1.7)	700 (2.0)	722[b] (3.0)
	300	844 (1.3)	830 (1.0)	700 (1.9)	720 (2.6)
2	100	836[a] (2.6)	817[a] (3.4)	705 (4.8)	733 (3.6)
	200	839[a,b] (2.4)	822[a] (4.1)	716 (3.6)	739[b] (4.5)
	300	842[a] (1.6)	827[a] (2.6)	718 (2.7)	738 (3.0)

[a] Fig. 11 shows one of the three time series on which this value is based.
[b] Fig. 12a shows the three time series on which this value is based.

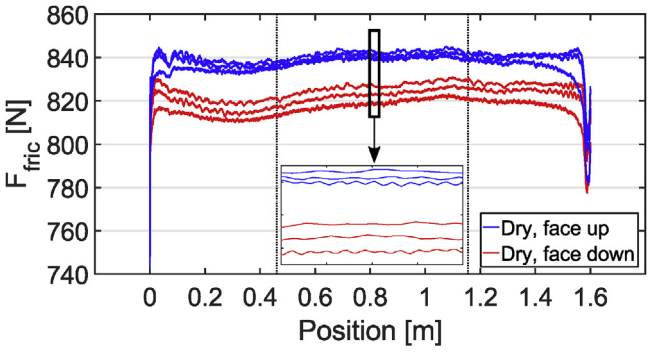

Fig. 11. Friction force during dry, dynamic tests in two orientations (face up, face down) as function of disc position for $L' = 2$ mm at three pull velocities: 100 mm/s, 200 mm/s, and 300 mm/s. The zoomed section shows the velocity dependence of the friction force; a higher friction corresponds to a higher velocity.

We will now highlight some results from Table 3 by looking at the time series on which the values in the table are based. Fig. 11 compares the dry face up and dry face down experiments for different velocities. The tubes that are squeezing the disc by 2 mm are used. The black dotted vertical lines indicate the range in which the discs are moving at constant speed. A slight velocity dependence is observed in the friction force. The zoomed section shows that higher velocities correspond to higher friction forces. The increase was, however, not significant. A maximum increase by 1.7% between 100 mm/s and 300 mm/s is found when looking at all experiments in Table 3. This means that in this parameter regime the value for the sliding friction can be regarded as approximately constant. At higher velocities, however, this may not be the case, as the friction coefficient will be dependent on the relative velocity of the sliding interfaces (Elmer, 1997). Fig. 11 and Table 3 show that higher friction forces are measured with the face up configurations, compared to the face down configurations. In the dry experiments the friction forces are higher by 0.5%–2.5%, while in the wet experiments the increase is 2.3%–3.9%. The difference in friction forces when comparing the face down and face up configurations can possibly be explained by a different chamfer on both sides of the sealing disc which introduces a asymmetry. Small changes in the size of the chamfer can have a significant effect on the force, as will be discussed in Section 3.4.

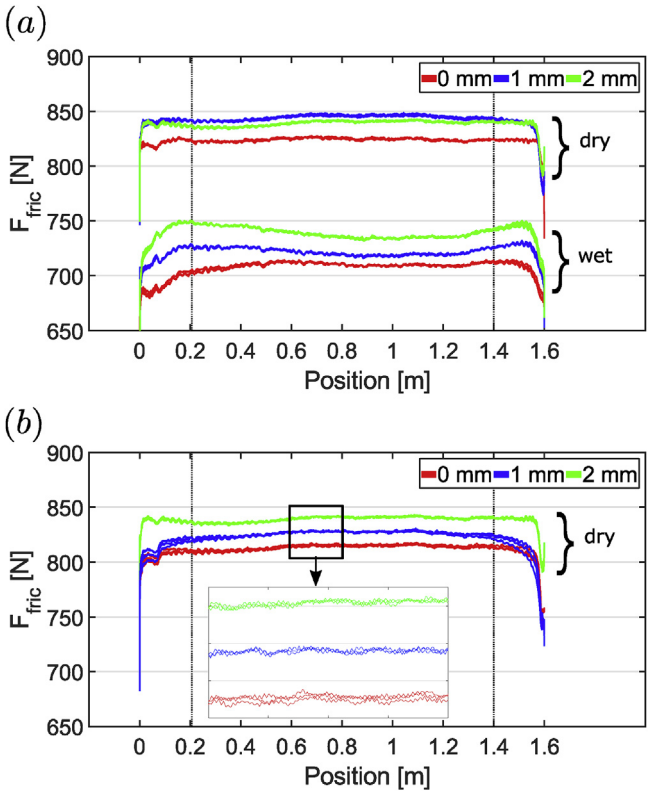

Fig. 12. (a) Friction force for three different pre-squeeze values and for two lubrication conditions. The pull velocity is 200 mm/s. (b) Friction force for three different pre-squeeze values; the experiments have been conducted directly after each other. The pull velocity is 200 mm/s.

Fig. 12a shows the results for the dry and wet experiments (both with a face up configuration) at 200 mm/s for the three values of L': 0, 1, and 2 mm. The effect of lubrication is clearly visible as the measured friction force for all the wet experiments is lower than for the dry experiments. Looking at the columns with the dry and the wet experiments in Table 3, the friction forces decrease between 12% and 16% in the wet experiments compared to the dry experiments. When focusing on the three curves of the wet experiments in Fig. 12a we note the following trend. An increase by 1.8% for the friction force is observed with 1 mm squeezing compared to the case without squeezing. A further increase by 2.4% is found when the squeezing is increased from 1 mm to 2 mm. This is equivalent to a total increase by 4.2% when the squeezing is increased from no squeezing to 2 mm squeezing in the wet runs at 200 mm/s. This leads to the conclusion that the increase in oversize caused by the clamping force, see Table 2, does increase the friction force.

When focusing on the dry experiments in Fig. 12a we observe an increase in friction force by 2.6% for the dry runs with 1 mm squeezing compared to the dry runs without squeezing. When increasing the squeezing from 1 mm to 2 mm in the dry runs, however, a slight decrease in friction force by 0.6% is observed. This is not expected as the increase in oversize due to the increase in L' is expected to increase the friction force further. This leads to the hypothesis that wear of the sealing disc was not negligible during the course of taking experiments with the different sets of tubes (equivalent to 600/3 = 200 m of pigging). The effect of wear is expected to decrease the friction force, which would oppose the increase in friction force due to increasing L'. To test this hypothesis an additional set of dry experiments is performed, in which the runs are performed directly after each other. All runs were conducted at a velocity of 200 mm/s; first five runs without squeezing, followed by five runs with 1 mm and 2 mm squeezing. The results are shown in Fig. 12b and in Table 4. The inset in Fig. 12b

Table 4
Dry runs performed with the three sets of tubes: 0 mm (no squeezing), 1 mm and 2 mm. The mean values of the force data are tabulated, averaged over the five runs and as found when the disc is moving at a constant velocity of 200 mm/s. Every run is repeated five times, corresponding to 50 m of pigging distance. Fig. 12b shows all force measurements.

L' [mm]	Friction force [N]
0	813
1	826
2	840

reveals the individual three time series on which the value in Table 4 is based. This shows excellent reproducibility for the subsequent runs.

Indeed the friction force increases when the disc is squeezed. An increase by 1.6% is observed with 1 mm squeezing compared to no squeezing and an increase by 1.7% for 2 mm squeezing compared to 1 mm squeezing. Thus a total increase by 3.3% with 2 mm squeezing compared to no squeezing. This confirms the hypothesis that wear is not negligible during the course of taking experiments with the different sets of tubes. Wear can only be approximately ignored when the runs are conducted directly after each other.

Indeed, wear is clearly visible upon inspecting the sealing disc. In Fig. 13 disc A is shown before using it in the dynamic experiments and after all experiments were conducted. It can be seen that the disc is fabricated with a certain chamfer on both sides. After completing all experiments, which means that the disc was used over a distance of approximately 1500 m, the chamfer has increased significantly to a length of 4 mm. In the next section the results of the dynamic experiments will be related to the static experiments as described in Section 3.2. The effect of the size chamfer in the translation from static experiments to the dynamic experiments will be discussed.

3.4. Relation between static and dynamic results

In Section 3.2 we have seen that the FE model is able to capture the results obtained in the static setup, using the E-moduli obtained in stress and strain tests without the use of any fitting parameters. It is however not possible to investigate the effect of a possible liquid film between the disc and the pipe wall on the friction factor with this setup, since the experiment is static. In the dynamic experiment it is however possible to investigate the presence of a liquid, as was shown in section 3.3. The next step is to relate the static results to the dynamic experiments. Both experiments measure the friction force, although the wall normal force cannot be measured in the dynamic experiments. We therefore need to deduce μ for the dynamic experiments, using the

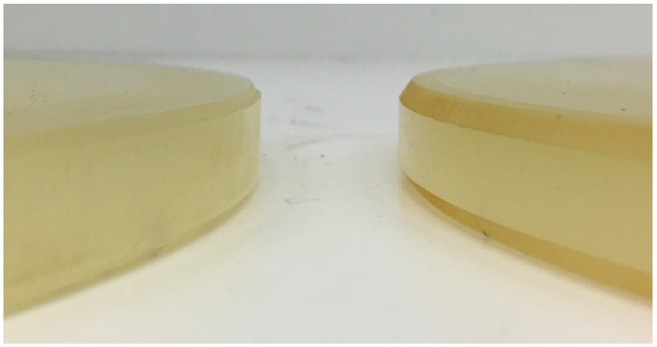

Fig. 13. The chamfers of disc A are shown. Disc A on the left is not used in the dynamic experiments and reveals the chamfer of approximately 1.4 mm as built-in by the manufacturer. On the right disc A is shown which is used in the dynamic experiments. The wear is clearly visible and the chamfer is 4 mm.

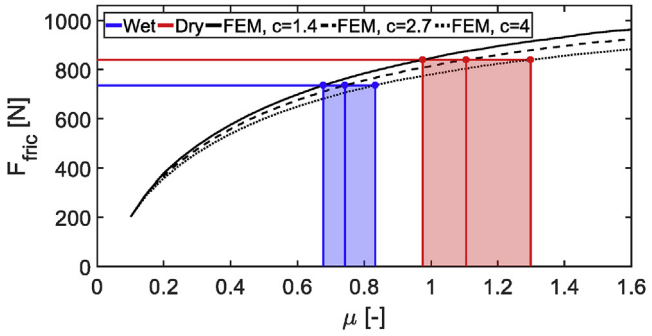

Fig. 14. Prediction of the μ values in the dynamic experiment, using three values of the chamfer length c. Using the FE results, the force data from the dynamic experiments are translated into μ values. μ is predicted between 0.97 and 1.30 in the dry runs and between 0.68 and 0.83 in the wet runs.

results from the static experiments.

Fig. 14 shows the FE prediction of μ for the dynamic experiments, using three values of the chamfer length c. Here the results of the FE model are shown in a similar way as in Section 3.2, but now for an oversize of 4.04%. In the static experiments with disc A the tubes were not yet used, but the circumference of the disc after clamping was measured. This circumference corresponds exactly to the circumference of disc A when squeezed by 2 mm in the dynamic experiments. Therefore this oversize was chosen, see Table 2.

When averaging the friction force for the different speeds for the dry experiments with $L' = 2$ mm (Table 3), a value of 839 N is found. Based on this value a corresponding μ value can be determined using the FE model. Wear was observed during the course of performing the dynamic experiments and it was found to increase the chamfer length c, see Fig. 13. To investigate the sensitivity of the chamfer size on the frictional force the FE calculations were performed with three different chamfer lengths: the original chamfer length c= 1.4 mm, the final chamfer length c= 4 mm, and an intermediate chamfer length c= 2.7 mm. It can be observed that the friction force decreases when the chamfer length increases, as it is easier to subject the sealing disc to 4.04% oversize when the chamfer is larger. This is in line with other research and a consequence is that the required driving pressure needed to propel the pig decreases throughout the course of a pigging run (Zhang et al., 2017). When we focus on a fixed value of 839 N for the friction force in the dry experiments, we thus find different μ values, ranging between $\mu = 0.97$ and $\mu = 1.30$. The wet experiments correspond to lower friction values, see Section 3.3, and therefore lower corresponding μ values are found, see Fig. 13. The results are summarized in Table 5. In the wet contact μ decreases by approximately 30%. An interesting follow-up experiment could be to use a biological or mineral oil as lubricant in the dynamic pig pull experiments.

Table 5
Force ratio μ versus the chamfer length c. Dry runs performed with the three sets of tubes: 0 mm (no squeezing), 1 mm and 2 mm. The mean values of the force data are tabulated, averaged over the five runs and as found when the disc is moving at a constant velocity of 200 mm/s. Every run is repeated five times, corresponding to 50 m of pigging distance. Fig. 12b shows all force measurements.

c [mm]	μ [−], dry	μ [−], wet
1.4	0.97	0.68
2.7	1.11	0.75
4.0	1.30	0.83

4. Conclusions

A static and dynamic experimental setup have been designed to investigate the frictional behaviour of a sealing disc of a pipeline pig. The static setup has been used to systematically study the effect of various parameters including the oversize, force ratio, thickness and E-modulus. In this way the study contributes to the fundamental knowledge on parameters influencing the friction force in pigging applications.

A finite element (FE) model was built which was able to accurately capture the behaviour of the experiments. The finite element model was able to accurately describe the static experiments, by using E-moduli obtained in stress and strain tests and without using any fitting parameters. When similar forces as measured in the experiment are acting on the chamfer in the finite element model, the maximum deformation varies by less than 2 mm for μ values larger than 0.25. Furthermore, the shapes obtained in the experiments agree very well with the shapes obtained with the finite element model. In the current experiment and FE model axisymmetry applies. For future research it could be interesting to investigate the effect of gravity which would break the axisymmetry. This effect is expected to become important when the gravitational forces become comparable with the forces which are purely caused by confining the sealing discs in the pipe.

When the disc is brought to a specific oversize between 1% and 4% in the finite element model, the required forces agree very well with the experimental force data. The maximum deviations for disc A and B occurred at 4% oversize. Here the finite element model underpredicts the friction force by a maximum of 5.2% and 11.6%, respectively. It is hypothesized that this underprediction is explained by undesired friction between the hull and the frame in the experimental setup, which is especially observed at high frictions forces. To test if this hypothesis is correct a setup could be designed which has more roller bearings between the hull and the frame which would result in even less friction.

The dynamic pig pull facility has been used to test the frictional behaviour during a dynamic pull test through a 1.7 m pipe for both a dry and a wet contact. This dynamic setup is complementary to the static pig pull facility. The influence of the clamping force of the spacer discs on the sealing disc diameter and frictional force has been investigated. It was found that by increasing the clamping force the diameter, and therefore the oversize, of the sealing disc increases. As a result the frictional force was found to increase during the dynamic pull tests. The largest difference in friction force is observed when comparing the dry and the wet experiments. Lubrication was clearly visible in the force measurements. Using water as a lubricant resulted in a decrease in the friction force by between 12% and 16% for the experiments conducted. This decrease in friction force is attributed to a difference in friction coefficient, which has been quantified using FE calculations. The sensitivity of the size of the chamfer in this analysis has been taken into account. This has led to a prediction of the friction coefficient of between 0.97 and 1.30 for a dry contact and of values between 0.68 and 0.83 for a wet contact. Only water has been used as lubricant in the experiments. It is suggested for future research to study also other lubricants, such as for example mineral oil.

Acknowledgments

The work by the first author was funded by Shell Projects & Technology, for which they are greatly acknowledged. The experiments were carried out in the lab of the Shell Technology Centre in Amsterdam. Thanks are due to Patrick van Holst and Harry Jansen for their help with the material tests. Thanks are also due to Ruud Henkes, Wim-Paul Breugem, Maurice Fransen, Peter Veenstra and Harry Gussekloo who helped to prepare and discuss the experiments.

Appendix A. Material tests

The Shore hardness is a sealing disc material property. It is a measure of the resistance of a material to indentation. For sealing discs the ASTM D2240 type A scale is used to measure the Shore hardness. Typical values of the Shore hardness A of a sealing disc are in the range: 60–85 ((Cordell and Vanzant, 2003)). The discs used in this report are specified by a Shore hardness of 75. The results are shown in Table A.6. The hardness tests were performed on the inner and outer diameters of the discs at ten different positions. The results for the disc A are within the specifications of the manufacturer, but the results for disc B are slightly higher.

Table A.6
Measured values of the Shore hardness A.

Sample#	Disc A		Disc B	
	Inner diameter	Outer diameter	Inner diameter	Outer diameter
1	75	76	81.5	81
2	75	75	80.5	79.5
3	74.5	74	80.5	79.5
4	74.5	74	80.5	79
5	74	74.5	80	78
6	76.5	75.5	79	80.5
7	76	75.5	79	79.5
8	75.5	75	79	79
9	75	74.5	79	78.5
10	75.5	75	79	79
Avg.	75.2	74.9	79.8	79.4
Std. Deviation	0.75	0.66	0.92	0.88

An important input parameter for the deformation models discussed in this report is the Young's modulus, also called the elastic modulus or E-modulus; vendors of sealing discs do not specify the E-modulus. There are ways to obtain the E-modulus from the Shore hardness, for example by using Gent's relation. In this research, however, it was chosen to determine the E-modulus by stress-strain tests. From the sealing discs a dog bone is cut using a bandsaw. Each dog bone was tested five times with a universal testing machine, see Figure A.15. One test consists of the following steps:

1. Uniform extension of 10 mm in 2 min
2. Two minutes rest in extended position
3. Uniform compression of 10 mm in 2 min to starting position

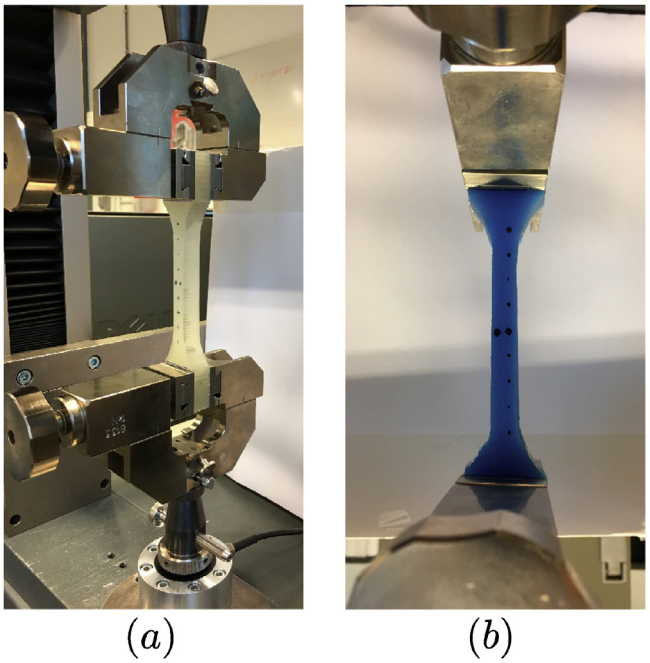

Fig. A.15. Universal testing machine. (a) Dog bone disc A. (b) Dog bone disc B.

During a test the tensile force F and the displacement ΔL are recorded with a frequency of 10 Hz. Using F and ΔL, the stress σ and strain ε are determined:

$$\sigma = \frac{F}{A} \tag{A.1}$$

$$\varepsilon = \frac{\Delta L}{L} \tag{A.2}$$

where A is the cross-sectional area in the thin region where the dog bone will stretch mostly and L is the starting length of the dog bone between the specimen holding jaws (here 11.2 cm). The E-modulus is determined by using Hooke's law:

$$E = \frac{\Delta\sigma}{\Delta\varepsilon} \tag{A.3}$$

Figure A.16 shows the E-modulus as function of the tensile strain for disc A and disc B, respectively. The E-modulus of the disc B is significantly higher than that of disc A. Both materials show a non-linear behaviour and the E-modulus decreases as the strain increases. This non-linearity is most apparent for the disc B when the strains exceed 0.04 mm/mm.

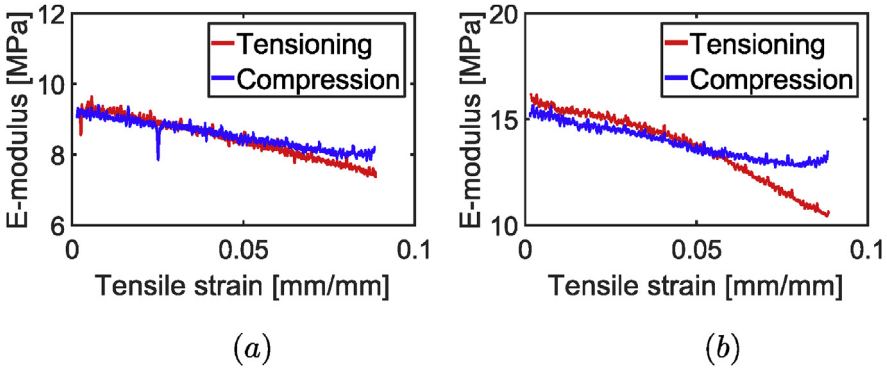

Fig. A.16. The E-modulus as a function of the tensile strain. (a) Disc A. (b) Disc B.

The E-modulus is used as input parameter in the finite element model; it will be a constant, which is equal to the average value of the E-moduli obtained in the five stress-strain tests per dog bone. In our stress-strain tests the displacement increases to 9% of the starting length as higher strains are unlikely to be encountered.

References

Carvalho, M.H.P., Rotava, E., 2017. Planning and execution of pigging procedure for gas pipeline. In: Offshore Technology Conference (28063), pp. 1–8.

Cordell, J., 1992. Conventional Pigs - what to Use and Why. Pipes and Pipelines International.

Cordell, J., Vanzant, H., 2003. The Pipeline Pigging Handbook, third ed. Clarion Technical Publishers & Scientific Surveys Ltd. ISBN: 0-9717945-3-7.

Elmer, F.-J., 1997. Nonlinear dynamics of dry friction. J. Phys. Math. Gen. 30 (17), 6057–6063.

Entaban, A., Ismail, A., Jambari, M., Ting, P., Amin, K.M., Ping, C., Zou, S., Van Spronsen, G., 2013. By-pass pigging - a 'simple' technology with significant business impact. In: Society of Petroleum Engineers - International Petroleum Technology Conference 2013, vol. 5. IPTC, pp. 3666–3671.

Esmaeilzadeh, F., Mowla, D., Asemani, M., 2009. Mathematical modeling and simulation of pigging operation in gas and liquid pipelines. J. Petrol. Sci. Eng. 69 (1–2), 100–106.

Gent, A., 1958. On the relation between indentation hardness and young's modulus. Rubber Chem. Technol. 31 (4), 896–906.

Hendrix, M.H.W., Den Heijer, A., Breugem, W.-P., Henkes, R.A.W.M., 2016. Frictional forces during pigging of multiphase pipelines. In: BHR Group - 10th North American Conference on Multiphase Technology (103), pp. 103–114.

Hendrix, M.H.W., Liang, X., Breugem, W.-P., Henkes, R.A.W.M., 2017. Characterization of the pressure loss coefficient using a building block approach with application to by-pass pigs. J. Petrol. Sci. Eng. 150 (2), 13–21.

Lan, Z., Liu, S., Xiao, H., Wang, D., 2017. Frictional behavior of wax–oil gels against steel. Tribol. Lett. 65 (3), 88.

Money, N., Cockfield, D., Mayo, S., Smith, G., 2012. Dynamic speed control in high velocity pipelines. Pipeline Gas J. 239 (8), 30–38.

Nieckele, A.O., Braga, A.M.B., Azevedo, L.F.A., 2001. Transient pig motion through gas and liquid pipelines. J. Energy Resour. Technol. Trans. ASME 123 (2–4), 260–268.

O'Donoghue, A., 1996. On the Steady Motion of Conventional Pipeline Pigs Using Incompressible Drive media. Ph.D. thesis. Cranfield University.

Persson, B., 1998. Sliding Friction. ISBN: 3-540-63296-4. Springer.

Quarini, J., Shire, S., 2007. A review of fluid-driven pipeline pigs and their applications. J. Process Mech. Eng. 221 (1), 1–10.

Rui, Z., Han, G., Zhang, H., Wang, S., Pu, H., Ling, K., 2017. A new model to evaluate two leak points in a gas pipeline. J. Nat. Gas Sci. Eng. 46 (36), 491–497.

Rui, Z., Wang, X., Zhang, Z., Lu, J., Chen, G., Zhou, X., Patil, S., 2018. A realistic and integrated model for evaluating oil sands development with steam assisted gravity drainage technology in Canada. Appl. Energy 213 (7), 76–91.

Singh, A., Henkes, R.A.W.M., 2012. CFD modelling of the Flow Around a By-pass Pig. In: 8th North American Conference on Multiphase Technology, vol. 16. pp. 229–243.

Tan, G., Wang, D., Liu, S., Wang, H., Zhang, S., 2013. Frictional behaviors of rough soft contact on wet and dry pipeline surfaces: with application to deepwater pipelaying. Sci. China Technol. Sci. 56 (12), 3024–3032.

Tan, G.-B., Wang, D.-G., Liu, S.-H., Zhang, S.-W., 2014. Probing tribological properties of waxy oil in pipeline pigging with fluorescence technique. Tribol. Int. 71 (4), 26–37.

Tan, G.-B., Liu, S.-H., Wang, D.-G., Zhang, S.-W., 2015. Spatio-temporal structure in wax-oil gel scraping at a soft tribological contact. Tribol. Int. 88 (27), 236–251.

Tiratsoo, J., 1992. Pipeline Pigging Technology, second ed. Gulf Professional Publishing ISBN: 0-8720142-6-6.

Tolmasquim, S.T., Nieckele, A.O., 2008. Design and control of pig operations through pipelines. J. Petrol. Sci. Eng. 62 (3–4), 102–110.

Wang, Q., Sarica, C., Volk, M., 2008. An experimental study on wax removal in pipes with oil flow. J. Energy Resour. Technol. Trans. ASME 130 (4) 0430011–0430015.

White, M., Pierce, K., Acharya, T., 2017. A Review of Wax-formation/mitigation Technologies in the Petroleum Industry. Society of Petroleum Engineers, pp. 1–10 189447.

Wu, H.L., van Spronsen, G., 2005. Slug reduction with high by-pass pigs - a mature technology. In: 12th International Conference on Multiphase Production Technology, Barcelona (3), pp. 313–325.

Zhang, H., Sanchez, C., Liu, S., Zhang, S., Liang, H., 2017. Wear of a polyurethane rubber used in dry gas pipeline as inspection gauges. J. Nat. Gas Sci. Eng. 41 (4), 40–48.

Zhu, X., Wang, D., Yeung, H., Zhang, S., Liu, S., 2015a. Comparison of linear and non-linear simulations of bidirectional pig contact forces in gas pipelines. J. Nat. Gas Sci. Eng. 27 (17), 151–157.

Zhu, X., Zhang, S., Li, X., Wang, D., Yu, D., 2015b. Numerical simulation of contact force on bi-directional pig in gas pipeline: at the early stage of pigging. J. Nat. Gas Sci. Eng. 23 (14), 127–138.

Zhu, X., Wang, W., Zhang, S., Liu, S., 2017. Experimental research on the frictional resistance of fluid-driven pipeline robot with small size in gas pipeline. Tribol. Lett. 65 (2), 1–10.